Neurophotonics

Neurophotonics.SPIEDigitalLibrary.org

Correlation between volumetric oxygenation responses and electrophysiology identifies deep thalamocortical activity during epileptic seizures

Sven Gottschalk
Thomas Felix Fehm
Xose Luís Deán-Ben
Vassiliy Tsytsarev
Daniel Razansky

SPIE.

Sven Gottschalk, Thomas Felix Fehm, Xose Luís Deán-Ben, Vassiliy Tsytsarev, Daniel Razansky, "Correlation between volumetric oxygenation responses and electrophysiology identifies deep thalamocortical activity during epileptic seizures," *Neurophoton.* **4**(1), 011007 (2016), doi: 10.1117/1.NPh.4.1.011007.

Neurophotonics 4(1), 011007 (Jan–Mar 2017)

Correlation between volumetric oxygenation responses and electrophysiology identifies deep thalamocortical activity during epileptic seizures

Sven Gottschalk,[a,†] Thomas Felix Fehm,[a,b,†] Xose Luís Deán-Ben,[a] Vassiliy Tsytsarev,[c] and Daniel Razansky[a,b,*]
[a]Institute for Biological and Medical Imaging (IBMI), Helmholtz Center Munich, Ingolstaedter Landstrasse 1, 85764 Neuherberg, Germany
[b]Technical University of Munich, Faculty of Medicine, Ismaninger Str. 22, 81675 Munich, Germany
[c]University of Maryland School of Medicine, Department of Anatomy and Neurobiology, 20 Penn Street, HSF II, Baltimore, Maryland 21201, United States

Abstract. Visualization of whole brain activity during epileptic seizures is essential for both fundamental research into the disease mechanisms and the development of efficient treatment strategies. It has been previously discussed that pathological synchronization originating from cortical areas may reinforce backpropagating signaling from the thalamic neurons, leading to massive seizures through enhancement of high frequency neural activity in the thalamocortical loop. However, the study of deep brain neural activity is challenging with the existing functional neuroimaging methods due to lack of adequate spatiotemporal resolution or otherwise insufficient penetration into subcortical areas. To investigate the role of thalamocortical activity during epileptic seizures, we developed a new functional neuroimaging framework based on spatiotemporal correlation of volumetric optoacoustic hemodynamic responses with the concurrent electroencephalogram recordings and anatomical brain landmarks. The method is shown to be capable of accurate three-dimensional mapping of the onset, spread, and termination of the epileptiform events in a 4-aminopyridine acute model of focal epilepsy. Our study is the first to demonstrate entirely noninvasive real-time visualization of synchronized epileptic foci in the whole mouse brain, including the neocortex and subcortical structures, thus opening new vistas in systematic studies toward the understanding of brain signaling and the origins of neurological disorders. [DOI: 10.1117/1.NPh.4.1.011007]

Keywords: epileptic seizures; functional brain imaging; optoacoustic tomography; photoacoustics; thalamocortical loop; hemodynamic response function; 4-aminopyridine.

Paper 16029SSR received Jul. 6, 2016; accepted for publication Sep. 13, 2016; published online Oct. 5, 2016.

1 Introduction

Epilepsy is a neurological disorder resulting from abnormal neural synchronization that causes recurring seizures spreading across both cortical and subcortical brain areas. More than 1% of the world population experiences this condition at least once in a lifetime.[1] Epileptic seizures are clearly recognizable on electroencephalogram (EEG) recordings as they are usually accompanied by bilateral 3 to 4 Hz spike–wave discharges (SWDs). However, the underlying neural mechanisms of the seizures are not yet fully understood. It is well recognized that SWDs are generated by the synchronized activity in the thalamocortical loop since neither the neocortex nor different nuclei of the thalamus (TA) alone can sustain them.[2] To this end, accurate localization of the onset, spread, and termination of the epileptic seizures can greatly impact the advancement of efficient therapies.

Imaging techniques play a fundamental role in the understanding of abnormal epileptic activity in both preclinical models and clinical studies.[3,4] Noninvasive imaging modalities, such as functional magnetic resonance imaging (fMRI)[4] or diffusion optical tomography,[5] are capable of whole brain visualization of functional brain activity. However, they lack the spatial and/or temporal resolution for accurate characterization of the seizure dynamics. Other optical methodologies have further been used to localize cerebral cortex activity *in vivo*,[6] yet it remains challenging to apply those methods to visualize subcortical brain structures involved into the epileptic process. Recently, miniature endoscopic probes have offered a potential alternative for imaging deep brain areas not accessible by intravital microscopy.[7] Yet, those approaches are only capable of simultaneous recordings from very limited areas while their inherent invasiveness may further alter the brain activity.

The vast growth in the development and application of optoacoustic imaging techniques has recently offered a viable alternative for high resolution deep brain observations. In contrast to optical microscopy and tomography techniques, whose penetration and resolution are severely hampered by strong light scattering in living tissues, optoacoustics is based on a direct transduction of light energy into ultrasonic waves, thus it enables mapping optical absorption with ultrasonic resolution not affected by light diffusion. The rich and spectrally distinctive hemoglobin-based optoacoustic contrast has resulted in a remarkable performance in label-free visualization of tissue hemodynamics,[6,8] stimulus-induced function, and brain metabolism.[9,10] Furthermore, by detecting spectroscopic changes in genetically encoded calcium indicators, functional optoacoustic

*Address all correspondence to: Daniel Razansky, E-mail: dr@tum.de

†Equal contribution

2329-423X/2016/$25.00 © 2016 SPIE

neurotomography has shown promise for direct monitoring of fast neural activity.[11] To this end, optoacoustic microscopy and tomography have been successfully employed to monitor brain hemodynamic responses due to electrical stimulation[9,12] and superficial seizure activity in mice.[13–15] Real-time optoacoustic imaging of two-dimensional (2-D) cross-sections through the whole mouse brain is further possible with systems based on arrays of cylindrically focused transducers.[16,17] However, efficient real-time volumetric optoacoustic visualization of epileptic seizures has not yet been achieved due to insufficient spatiotemporal resolution in three-dimensions (3-D) and lack of fast whole-brain imaging capacity.

In the current study, we devised a new multimodal functional neuroimaging framework based on temporal correlation between the whole-brain functional hemodynamic responses imaged by real-time volumetric optoacoustics and electrophysiological recordings. The ability of the suggested approach to non-invasively visualize real-time thalamo-cortical activity is investigated by inducing epileptic seizures by intracranial injection of 4-aminopyridine (4-AP) into the mouse neocortex.

2 Methods

2.1 *Animal Preparation*

Eight- to twelve-week-old female athymic nude-Foxn1^{nu} mice (Harlan Laboratories LTD, Itingen, Switzerland) were used in our *in vivo* experiments, which were performed in full compliance with the institutional guidelines of the Institute for Biological and Medical Imaging and with approval from the Government District of Upper Bavaria. The animals were anesthetized with isoflurane (2.5% v/v for induction and surgery) in 100% O_2 and fixed into a custom designed stereotactic mouse head holder (Narishige International Limited, London, United Kingdom) to avoid head motion. They were subsequently placed into a robot stereotactic drill and injection system (Neurostar, Tuebingen, Germany), where the scalp was removed. During all surgical procedures, hemostatic sponges (Gelfoam®, Pfizer Pharmaceutical) were used along with a topical application of adrenaline to minimize bleeding.[18] Next, two small holes were drilled into the skull, one posterior and one laterally, by using a handheld surgical drill (Ideal Micro-Drill, Harvard Apparatus, Holliston, Massachusetts). Two stainless steel screw electrodes were then implanted for the EEG recordings (Fig. 1). An additional (smaller) hole for intracranial injection was drilled laterally to the superior sagittal sinus (SSS) and on the same side, where the EEG screws were located. During the experiments, physiologic parameters—including blood oxygenation, heart rate, and body temperature—were continuously tracked using the PhysioSuite physiological monitor (Kent Scientific, Torrington, Connecticut). The body temperature was kept constant using a rectal thermometer and a feedback-controlled heating pad (PhysioSuite, Kent Scientific, Torrington, Connecticut), while the animals were maintained under isoflurane anesthesia with 1.0% to 1.5% v/v in 100% O_2 with a flow rate of ~0.7 L/min. The EEG signal was recorded by means of an AC/DC differential amplifier (Model 1700, A-M Systems, Sequim, Washington) and digitized at 1000 samples per second with a PC-embedded A/D converter (Model ATS9351, Alazar Technologies Inc., Pointe-Claire, Quebec, Canada).

2.2 *Epilepsy Model*

The potassium channel blocker 4-AP model of epileptic seizures has been shown to allow for reproducible studies of abnormal neural synchronization using different electrophysiological and imaging methods.[19,20] 4-AP inhibits the K^+ outward current, which, in turn, causes prolongation of action potentials and abnormal neural synchronization.[19] This model can generate focal seizures lasting up to hundreds of seconds with interictal periods of minutes for a duration of several hours.[15] In contrast to generalized models of epilepsy, which lead to a more widespread (global) activation in the entire brain,[13] the 4-AP model allows better characterization of the onset and spread of localized epileptic seizures. In our study, 0.6 μL of 25 mM 4-AP dissolved in artificial cerebrospinal fluid (ACSF) were injected intracranially by a robot injection system (Neurostar, Tuebingen, Germany) using a 15 to 25 μm diameter glass microcapillary. Injections were made ~0.5 mm below the dura mater surface into the neocortex. As control, the vehicle ACSF was injected in the same way. After injection, the animal with the mounted head holder was transferred into the imaging setup.

2.3 *Optoacoustic Tomography System*

The general methodology for real-time acquisition of multispectral volumetric optoacoustic data has been described elsewhere.[8,21,22] In brief, optoacoustic signals were excited using a nanosecond-pulsed optical parametric oscillator laser source (SpitLight, Innolas Laser GmbH, Krailling, Germany). The laser can be operated with up to 100-Hz pulse repetition frequency and provides a unique fast tuning capability allowing for switching the illumination wavelength on a per-pulse basis within the entire near-infrared spectrum (690 to 950 nm). The excitation light was guided to the mouse head using a custom-made fiber bundle (CeramOptec, Bonn, Germany), which delivers a ~10-mm diameter Gaussian illumination profile at the skull surface. The per-pulse energy at the fiber output was kept below 15 mJ. The generated optoacoustic responses were collected at different locations around the imaged volume by means of a custom-made 256-element spherical matrix detection array (Imasonic SaS, Voray, France) and simultaneously digitized with a custom-made parallel data acquisition system (Falkenstein Mikrosysteme GmbH, Taufkirchen, Germany). In the experiments, image data at five excitation wavelengths (700, 730, 750, 800, and 850 nm) were acquired. Data acquisition was controlled through a host PC using a custom-designed MATLAB®-based graphical user interface (Version 2013a, Mathworks Inc., Natick, Massachusetts).

2.4 *Data Processing and Image Reconstruction*

The data acquisition and processing pipeline is summarized in Fig. 1. The acquired optoacoustic signals were first deconvolved with the impulse response function of the array detection elements to account for their limited detection bandwidth. The signals were subsequently bandpass filtered using a Butterworth frequency filter between 0.1 and 6 MHz to remove low frequency drifts as well as high frequency noise. Optoacoustic image reconstruction was then performed on a Cartesian grid by means of a GPU-based implementation of a filtered backprojection algorithm[23,24] for every wavelength using a volumetric image grid of $100 \times 100 \times 100$ voxels. Intensity variations due to fluctuations in the laser energy were compensated by normalizing

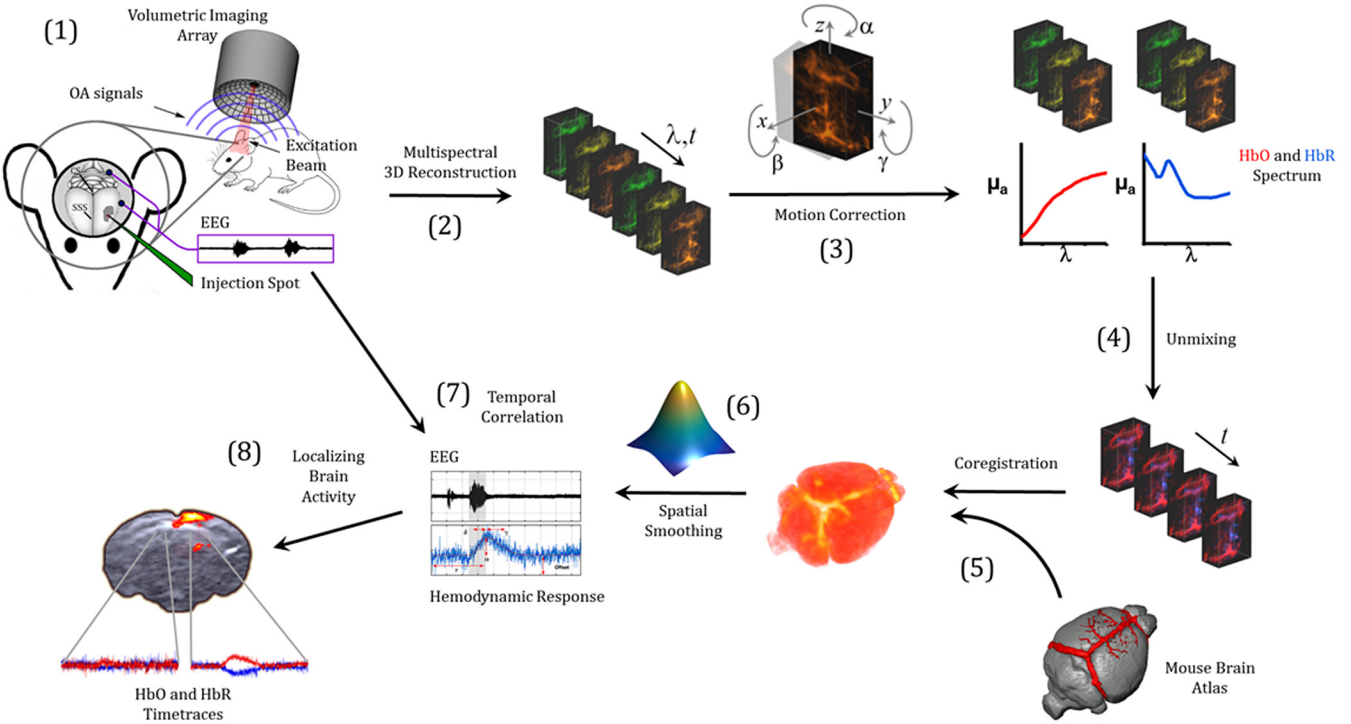

Fig. 1 Real-time volumetric imaging of hemodynamic changes in the brain, concurrent EEG readings and temporal correlation processing pipeline. (1) Epileptic seizures are induced by intracranial injection of 4-AP into the neocortex of the mouse brain (green solid arrow). The outline of the mouse brain is indicated with two major vasculature features (SSS: superior sagittal sinus, CS: confluence of sinuses). EEG is recorded through screw-type electrodes implanted into the skull as indicated (black circles). Optoacoustic (OA) signals are generated by pulsed laser excitation and detected by means of a volumetric imaging array. (2) Multispectral optoacoustic three-dimensional (3-D) images are first reconstructed for each wavelength and time-point. (3) To compensate for breathing and spastic motion, linear and rotational affine transformations are implemented for each reconstructed frame. (4) Next, spectral unmixing is performed using the known absorption spectra of oxygenized (HbO) and deoxygenized (HbR) hemoglobin, generating 3-D maps representing their spatial distribution. (5) These maps are then coregistered to standardized brain atlases representing the average vascular morphology of the mouse brain as well as the spatial sectioning of known brain regions. (6) After applying a Gaussian filter for spatial smoothing of the maps, (7) temporal correlation between the real-time 3-D hemodynamic optoacoustic responses and the concurrent EEG-readings is performed. (8) By this, hemodynamic changes representing neural activity can be localized by fitting the optoacoustic hemodynamic response function to the time trace of each voxel. The performed coregistration allows then to identify active regions of the brain.

every reconstructed volume with the average optoacoustic signal recorded from a small rod-shaped absorber positioned between the fiber outlet and the mouse head.

2.5 *Motion Correction*

Breathing and spastic motion of the mouse may adversely affect the accuracy of unmixing algorithms in multispectral optoacoustic tomography.[25] Herein, the relative motion between optoacoustic images acquired at five different wavelengths was accounted for by implementation of a dedicated motion correction framework. For the first multispectral dataset, the reconstructed image volume at 800 nm was selected as a reference while the images at the remaining wavelengths were reoriented to match their position and orientation using 3-D rigid-body transformations. The motion-corrected frames for each wavelength were then used as references for all subsequent frames acquired at the same wavelengths. Volumetric co-registration was implemented in MATLAB® 2013a using the available affine transformation package. The necessary parameters were estimated using the "imregtform" function with the search space limited to linear translations and rotations only.

2.6 *Spectral Unmixing*

The 3-D maps representing the spatial distribution of oxygenated and deoxygenated hemoglobin were calculated for every time instant using the motion corrected volumes of every set of wavelengths assuming a linear mixing model.[26] Specifically, for every voxel (x, y, z) and time instant t, the reconstructed optical absorption value at each wavelength I_j was modeled as a linear superposition of oxygenated (HbO) and deoxygenated hemoglobin (HbR) as well as additional noise term N, i.e.,

$$\begin{pmatrix} I_1 \\ \vdots \\ I_5 \end{pmatrix} = \begin{bmatrix} \varepsilon_1(\lambda_1) & \cdots & \varepsilon_3(\lambda_1) \\ \vdots & \ddots & \vdots \\ \varepsilon_1(\lambda_5) & \cdots & \varepsilon_3(\lambda_5) \end{bmatrix} \begin{pmatrix} \mathrm{HbO} \\ \mathrm{HbR} \\ N \end{pmatrix}. \quad (1)$$

The extinction coefficients ϵ correspond to the known absorption spectra for oxygenated and deoxygenated hemoglobin,

while a constant arbitrary value was assumed for the noise channel. The intensity values of HbO, HbR, and N were then retrieved by calculating the Moore–Penrose pseudoinverse of the extinction coefficient matrix. Note that the linear unmixing approach may suffer from inaccuracies due to wavelength-dependent light attenuation thus generating quantitative errors when it comes to estimating the spatial distribution of oxygenated and deoxygenated hemoglobin, especially in deep tissues.[27] However, we are primarily interested in the relative temporal dynamics of the oxygenation profiles and the corresponding delays in the thalamocortical loops, which are not affected by the quantitative errors in estimating the chromophore concentrations.

2.7 *Anatomical Image Registration*

The imaging system used in the current study provides true 3-D information, which readily allows for coregistration with known mouse brain atlases. This is in contrast to cross-sectional optoacoustic tomographic imaging systems that have been previous employed for imaging the brains of rodents, which suffer from out-of-plane artifacts and highly anisotropic resolution, especially in the depth dimension.[16,17] The unmixed HbO and HbR maps were coregistered with two standardized brain atlases representing the average vascular morphology in a mouse brain[28] and the spatial sectioning of the known mouse brain regions,[29,30] respectively, both of which are available online (Ref. 31). First, fiducial markers were estimated manually for a single imaging frame using known well-resolved structures of the brain atlas as well as dominant vasculature features in the reconstructed optoacoustic volumes, which were all visible parts of the SSS, the confluence of sinuses, the longitudinal hippocampal vein descending from the confluence, and both transverse sinuses connected to the confluence. The estimated coregistration parameters for isotropic scaling, rotation, and translation were then used to automatically coregister all remaining frames in the time series using the standard affine transformation package available in MATLAB® 2013a.

2.8 *Localization of Epileptic Activity*

Finally, active voxels were identified in the coregistered oxygenation maps by Gaussian modeling of an optoacoustic hemodynamic response function (OHRF) for both the HbO and HbR channels. Much like the blood oxygenation level dependent (BOLD) response in fMRI data, the OHRF is affected by changes in blood flow, more specifically by the associated changes in blood volume and hemoglobin concentration, and by changes in oxygen saturation corresponding to oxygen consumption. However, since the origin as well as the underlying physiological and biophysical background of the optoacoustic signals are fundamentally different from the MR responses, the OHRF model is not based on the well-established models for the BOLD signal. Instead, similar to hemodynamic response functions that are used for the analysis of fMRI data,[32] we devised the OHRF to identify thalamocortical activity from empirical findings of the current study for voxels, where hemodynamic changes associated with neuronal activation were identified (Fig. 2). Assuming that the temporal response of every voxel $T(t)$ can be modeled with independent characteristic onset and offset time constants for neuronal activity, one may express it as

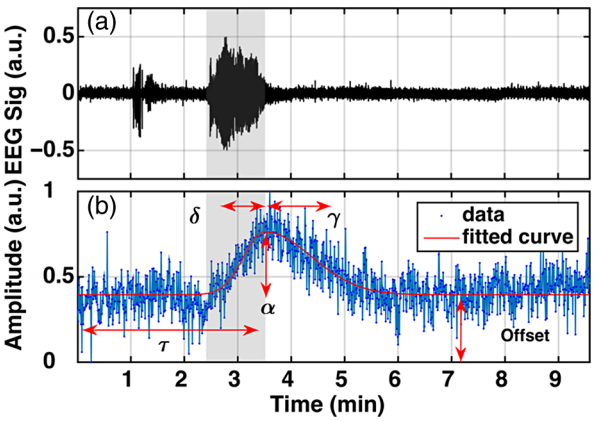

Fig. 2 Model employed in this study to identify active voxels. (a) EEG as it was measured during one of the experiments—periods of epileptic seizures can clearly be discerned (gray area) from background neuronal activity. (b) The optoacoustic hemodynamic responses were modeled with the following function: $T(t) = \alpha\,\{\Theta(t-\tau)\exp[-(t-\tau/\gamma)^2] + \Theta(\tau-t)\ \exp[-(t-\tau/\delta)^2]\} + \text{Offset}$.

$$T(t) = \alpha\left\{\Theta(t-\tau)\ \exp\left[-\left(\frac{t-\tau}{\gamma}\right)^2\right] + \Theta(\tau-t)\ \exp\left[-\left(\frac{t-\tau}{\delta}\right)^2\right]\right\} + \text{Offset}, \tag{2}$$

where $\Theta(t)$ is the Heaviside step-function. Specifically, it was found that the shape of the OHRF in either the HbO or the HbR channel can be approximated by Eq. (2), where τ coincides with the termination time of the seizure activity in the EEG; δ and γ represent the characteristic time constants of the rising and declining portions of the signal, respectively. The model was independently fitted to the time trace of each voxel and voxels were defined to be active if their corresponding parameters obeyed empirically derived constraints. Specifically, it was found that consistent results were obtained by constraining the relative change in amplitude α to be at least 15% of the fitted value for the offset. Signal traces were further constrained by rejecting signals with root mean square error ε of the fit larger than an empirically derived threshold. Also, potential false positives were suppressed by assigning voxels as active only if their corresponding fitted value for the termination time τ and the duration of the seizure δ lay within the seizure activity window as measured by the EEG. Before the fitting was performed, volumetric maps representing the spatial distribution of HbO and HbR at every individual time instant were smoothed by applying a Gaussian filter with a sigma of two voxels.

3 Results

Experiments were performed with anaesthetized animals placed under the volumetric optoacoustic tomography array. Generation of optoacoustic signals[33] was done by directing an unfocused beam of short-pulsed laser light in the near-infrared spectral region onto the mouse head. Real-time volumetric imaging of hemodynamic changes in the brain was performed by spectral unmixing of the reconstructed optoacoustic volumes at five different wavelengths in the near-infrared (see Fig. 1 and Sec. 2 for details of the signal acquisition and processing pipeline).

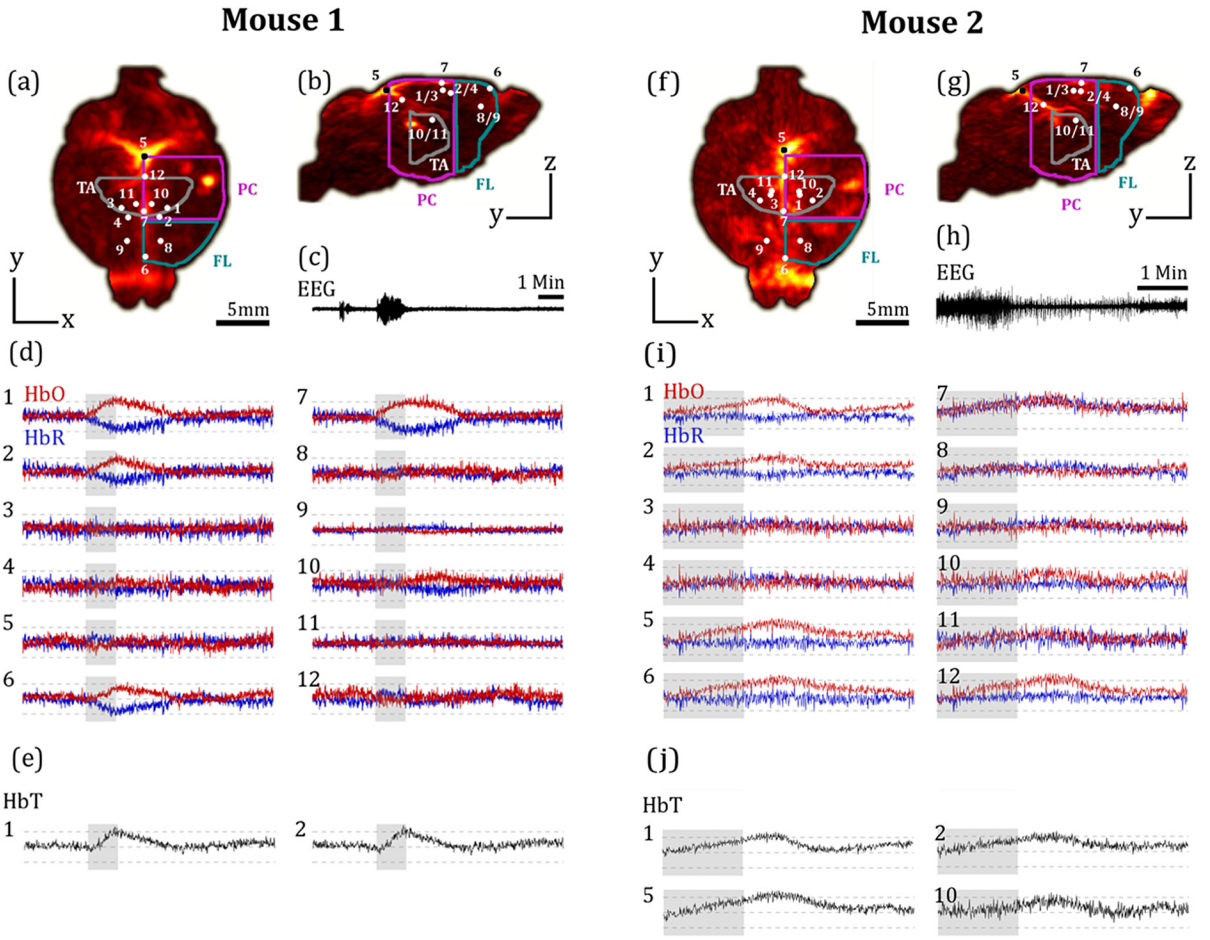

Fig. 3 Single voxel analysis of hemodynamic changes during epileptic seizures in two independent experiments (Mouse 1 and 2). (a and f) Maximum intensity projection (MIP) along the depth direction of HbO distribution in the mouse brain. Analyzed voxels are indicated and correspond to plotted time traces in (d and i). Colored outlines specify the location of brain regions (TA, gray: thalamus; PC, purple: parietal cortex; FL, green: frontal lobe). (b and g) Coronal MIP view of (a and f). (c and h) EEG. (d and i) Time traces of HbO (in red) and HbR (in blue) in the voxels shown in (a and f) and (b and g) are plotted. Gray boxes indicate the length of the seizure-associated neural activity as seen in the EEG. Dotted gray lines indicate averaged baseline and $\pm 50\%$ relative changes for each curve. (e and j) Total hemoglobin (HbT) was calculated from the signal intensities of HbO and HbR as HbT = HbO + HbR. HbT curves are only plotted for voxels with changes bigger than the background noise. The analyzed regions encompass the side of the brain, where 4-AP was injected and respective voxels in the contralateral (cl) side of the brain and inside major draining veins: Injection site (1 and 2) and (cl: 3, 4); superior sagittal sinus (6, 7); confluence of sinuses (5); longitudinal hippocampal vein (12); voxels anterior to the injection site (8, cl: 9); thalamus (10, cl: 11).

The particular advantage of our method is its unique ability to assess real-time changes in both oxygenized (HbO) and deoxygenized (HbR) hemoglobin in single voxels across the entire mouse brain. In experimental results, presented in Fig. 3, voxels in and around the injection site of 4-AP, i.e., the main epileptic focus, show concomitant increase and decline in HbO and HbR [traces 1 and 2 in Figs. 3(a), 3(b), and 3(d)], respectively, together with elevated EEG activity [Fig. 3(c)]. Note that the hemodynamic optoacoustic responses persist longer, as was previously observed with optical methods.[19] Significant increase in total hemoglobin (HbT) levels has further accompanied the hemodynamic changes in the focal area [Fig. 3(e)], most likely due to an increase in blood flow in the activated brain regions. Notably, analysis of voxels in the contralateral brain hemisphere at similar depths (traces 3 and 4) showed neither changes in HbO nor in HbR. However, a significant hemodynamic response was observed in the major draining vein, namely the SSS (Fig. 3, traces 6 and 7). The delayed onset of these changes in voxel 6 and the absence of fluctuations in voxels 5 and 12 (located in the confluence of sinuses and the longitudinal hippocampal vein, respectively) may suggest a link to the recently reported bidirectional flow effect in the SSS.[34] Analysis of deeper regions at anterior locations to the 4-AP injection site (traces 8 and 9) revealed no measurable changes, thus showing the final extent of the activated area in the cortex. On the other hand, similar analysis in the TA area demonstrated clear hemodynamic patterns temporally correlating with the EEG, although having generally lower magnitude as compared to the cortical activation areas (trace 10). It is important to notice that the activity inside the TA occurred at a later point with respect to the seizure-onset zone (traces 1 and 2), while neural activity inside the TA was arguably not visible in the EEG traces. Much like for the superficial cortical regions, no hemodynamic changes inside the contralateral side of the TA were detected (trace 11).

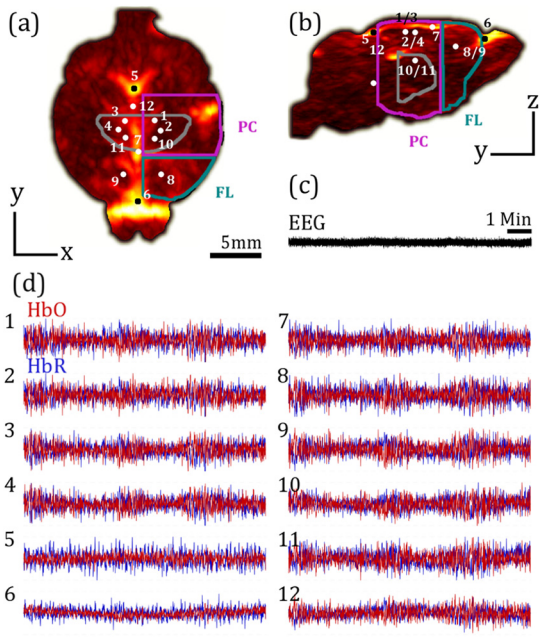

Fig. 4 Single voxel analysis of blood oxygenation in a control mouse showing typical background neural activity without epileptic seizures. (a) Maximum intensity projection (MIP) along the depth direction of HbO distribution in the mouse brain. Analyzed voxels are indicated and correspond to curves plotted in (d). Colored outlines specify the location of brain regions (TA, gray: thalamus; PC, purple: parietal cortex; FL, green: frontal lobe). (b) Coronal MIP view similar to (a). (c) EEG. (d) Time traces of HbO (in red) and HbR (in blue) in the voxels shown in (a) and (b) are plotted. For a detailed description of the voxel positions, see Fig. 3.

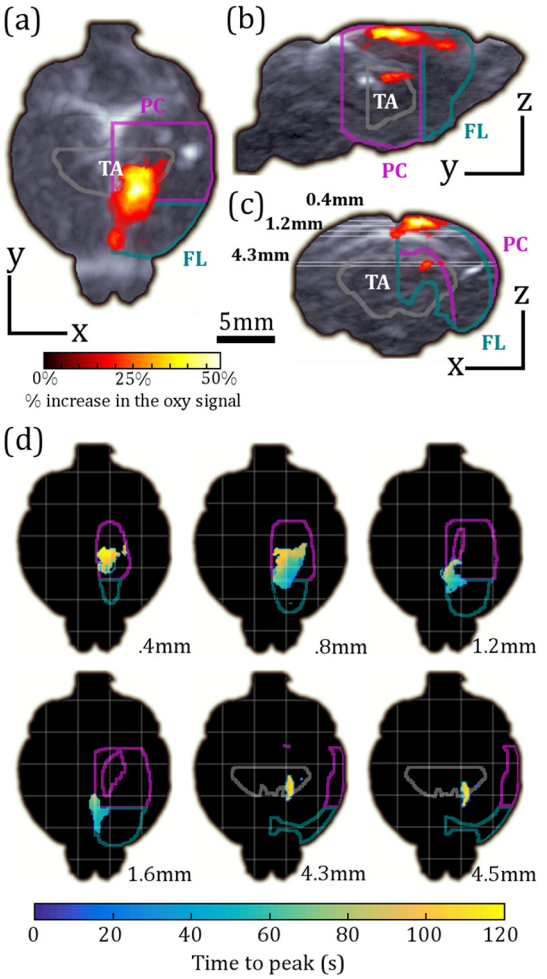

Fig. 5 Intensity plots of the seizure-related hemodynamic activity as identified by correlating the optoacoustic hemodynamic responses to the EEG traces. Maximum intensity projection views along the (a) horizontal, (b) sagittal, and (c) coronal directions of the brain of the neuronal activity pattern projected onto the corresponding volumetric optoacoustic reconstruction are shown. Spatial dimensions of the thalamus (TA, gray), the frontal lobe (FL, green) as well as the parietal–temporal cortex (PC, purple) are outlined. The correlation parameters are: 3 min $< \tau <$ 4 min, $\epsilon = 0.05$, $\alpha = 0.25\ \alpha_{\max}$ (see Sec. 2 and Fig. 2 for details). (d) Time to peak analysis of activated areas in the different transverse slices across the brain—the corresponding slice depth is indicated in (c).

In general, analysis of the other epileptiform events always revealed a high level of temporal correlation between the hemodynamic optoacoustic responses and the main surge of activation recognized in the EEG traces. Similar results from an independent experiment are shown in Figs. 3(f)–3(j). Strong hemodynamic responses in both HbO and HbR were again observed in the main epileptic focus together with EEG activity [traces 1 and 2 in Figs. 3(f)–3(i)]. This was again accompanied by changes in the major veins, however, mainly in HbO (traces 5, 6, and 12) together with increases in HbT [Fig. 3(j)]. Notably, the later onset of activity in the TA as compared to the cortex region was reproduced as well but also only in HbO (trace 10). Analysis of further voxels around voxel 10 showed a clear increase in HbO in a larger region in the TA (data not shown). Consistently, all hemodynamic changes persisted longer than EEG activity and neither significant hemodynamic responses were observed in the contralateral brain hemisphere nor at locations anterior to the 4-AP injection site (traces 3, 4, 11 and 8, 9 respectively).

Additionally, analysis of the optoacoustic and EEG data for a control mouse injected with the 4-AP vehicle ACSF showed neither detectable EEG activity nor hemodynamic changes over the entire duration of the experiment (Fig. 4).

Finally, in order to recognize 3-D spatiotemporal maps of the seizure propagation, we performed temporal correlation between the real-time 3-D hemodynamic optoacoustic responses and the concurrent EEG readings, according to the processing pipeline outlined in Sec. 2 and Fig. 1. The estimated seizure-related maps of hemodynamic activity are presented in Figs. 5(a)–5(c). Seizure-related hemodynamic changes can be readily recognized in the proximity of the 4-AP injection site in the left hemisphere of the parietal-temporal cortex (PC). Further concomitant neuronal activation occurs in the left frontal lobe (FL). The strongest activity pattern is detected close to the surface in the PC but extends into deeper structures within both the PC and FL. Hemodynamic changes further spread into the SSS. More importantly, the time to peak analysis [Fig. 5(d)] reveals a delayed onset of activity inside the TA. In particular, the activity arises first in the injection site of 4-AP in the boundary between PC and FL (transverse slices at depths of 0.8, 1.2, and 1.6 mm) and progresses further into the PC (slices at 0.4 and 0.8 mm depth). Activity inside the TA clearly occurs past the activity in the cortical regions and can be detected at depths of up to ~4.5 mm (slices 4.3 and 4.5 mm) from the brain surface.

4 Discussion and Conclusions

Accurate localization of epileptic seizures has great importance in advancing the understanding of the underlying mechanisms and hence in the development of antiepileptic therapies. The seizures frequently originate from oscillatory thalamocortical interactions that involve millions of neurons inside the thalamic nuclei and different areas of the sensory cortex.[35] In healthy brains, thalamocortical interactions are responsible for regulating the flow of information between the TA and cortical brain regions.[36] It was previously assumed that thalamic neurons change their inherent oscillatory properties in response to depolarization associated with different sensory and feedback inputs. Normally, these oscillations have frequencies of a few Hertz, but can change during pathological synchronizations in epileptic seizures.[37] However, systematic studies are often hindered by the fact that the underlying pathologies for focal epilepsy are distributed throughout different areas of the brain that cannot be simultaneously visualized with adequate spatiotemporal resolution using conventional functional neuroimaging techniques.

Here, we present a new functional neuroimaging framework based on spatiotemporal correlation of volumetric optoacoustic hemodynamic responses with the concurrent EEG recordings and anatomical brain landmarks. The method is demonstrated to be capable of accurate 3-D mapping of the onset, spread, and termination of the epileptiform events in 4-AP acute model of focal epilepsy. Of particular relevance is the deep brain optoacoustic imaging capability, which enables mapping the brain activity in regions inaccessible with high-resolution optical methods at an unprecedented temporal resolution. The presented results thus supplement electrophysiology studies of thalamocortical oscillations by providing temporally correlated 3-D imaging data of hemodynamic changes in the entire brain.

The 4-AP model of focal epilepsy used herein has been shown to mimic the characteristics of spontaneous chronic ictal activity in humans.[38] Specifically, the intracranial injection of 4-AP *in vivo* causes tonic–clonic focal seizures initiated at the injection location.[19] This is in good agreement with our volumetric hemodynamic observations as the maximum measured activity occurred close to the injection spot. On the other hand, it has been previously reported that epileptic seizures are accompanied by local changes in oxygenation and cerebral blood flow at the epileptic focus,[39,40] which was further confirmed by our results. The observed hemodynamic changes in 4-AP-induced seizures are also in good accordance with laser Doppler flowmetry and tissue oxygenation studies,[20] which revealed that the decrease in HbR around the main epileptic focus (i.e., close to the injection site) reflects a high oxygen consumption attributed to an increased seizure-associated neuronal activity.[20] At the same time, the measured changes in total hemoglobin concentration most likely reflect an increase in blood flow,[20,38] which is consistent with the natural physiological response of increased HbO supply into the activated area.

In conclusion, our work is the first to demonstrate entirely noninvasive real-time visualization of synchronized epileptic foci in the whole mouse brain, including the neocortex and subcortical structures, which is of key importance for systematic studies of epileptic seizures. The same methodology is readily applicable for characterization of different sensory responses (e.g., due to somatosensory, paw, or whisker stimulations) and can be further combined with the recently demonstrated optoacoustic imaging of fast neuronal responses using calcium indicators,[11] thus shedding more light on the mechanisms of neurovascular coupling and the origins of neurological disorders.

Acknowledgments

The authors acknowledge grant support from the European Research Council under grant agreements ERC-2010-StG_260991 and ERC-2015-CoG_682379. D.R, V.T., and S.G proposed and designed the project. T.F.F and X.L.D.B designed the optoacoustic imaging system. S.G, V.T., X.L.D.B., and D.R. carried out the experiments. T.F.F and X.L.D.B implemented image reconstruction and processing algorithms. T.F.F and S.G analyzed the data. D.R, S.G. and V.T. supervised the study. All authors discussed the results and contributed to writing the manuscript.

References

1. M. Trimble and D. C. Hesdorffer, "Representations of epilepsy on the stage: from the Greeks to the 20th century," *Epilepsy Behav.* **57**, 238–242.(2016).
2. M. Avoli, "A brief history on the oscillating roles of thalamus and cortex in absence seizures," *Epilepsia* **53**, 779–789, (2012).
3. D. N. Lenkov et al., "Advantages and limitations of brain imaging methods in the research of absence epilepsy in humans and animal models," *J. Neurosci. Methods* **212**, 195–202, (2013).
4. Z. L. Yang and L. J. Zhang, "PET/MRI of central nervous system: current status and future perspective," *Eur. Radiol.* **26**, 3534–3541 (2016).
5. H. Yang et al., "*In vivo* imaging of epileptic foci in rats using a miniature probe integrating diffuse optical tomography and electroencephalographic source localization," *Epilepsia* **56**, 94–100, (2015).
6. V. Tsytsarev, C. Bernardelli, and K. I. Maslov, "Living brain optical imaging: technology, methods and applications," *J. Neurosci. Neuroeng.* **1**, 180–192, (2012).
7. Q. Tang et al., "*In vivo* voltage-sensitive dye imaging of subcortical brain function," *Sci. Rep.* **5**, 17325, (2015).
8. S. Gottschalk et al., "Noninvasive real-time visualization of multiple cerebral hemodynamic parameters in whole mouse brains using five-dimensional optoacoustic tomography," *J. Cereb. Blood Flow Metab.* **35**, 531–535, (2015).
9. L. D. Liao et al., "Transcranial imaging of functional cerebral hemodynamic changes in single blood vessels using *in vivo* photoacoustic microscopy," *J. Cereb. Blood Flow Metab.* **32**, 938–951, (2012).
10. J. Yao et al., "High-speed label-free functional photoacoustic microscopy of mouse brain in action," *Nat. Methods* **12**, 407–410, (2015).
11. X. L. Dean-Ben et al., "Functional optoacoustic neuro-tomography for scalable whole-brain monitoring of calcium indicators," *Light Sci. Appl.* **5**, e16201, (2016).
12. V. Tsytsarev et al., "Photoacoustic microscopy of microvascular responses to cortical electrical stimulation," *J. Biomed. Opt.* **16**, 076002, (2011).
13. J. Tang et al., "Noninvasive high-speed photoacoustic tomography of cerebral hemodynamics in awake-moving rats," *J. Cereb. Blood Flow Metab.* **35**, 1224–1232, (2015).
14. V. Tsytsarev et al., "*In vivo* imaging of epileptic activity using 2-NBDG, a fluorescent deoxyglucose analog," *J. Neurosci. Methods* **203**, 136–140, (2012).
15. V. Tsytsarev et al., "Photoacoustic and optical coherence tomography of epilepsy with high temporal and spatial resolution and dual optical contrasts," *J. Neurosci. Methods* **216**, 142–145, (2013).
16. N. C. Deliolanis et al., "Deep-tissue reporter-gene imaging with fluorescence and optoacoustic tomography: a performance overview," *Mol. Imaging Biol.* **16**, 652–660, (2014).
17. M. Nasiriavanaki et al., "High-resolution photoacoustic tomography of resting-state functional connectivity in the mouse brain," *Proc. Natl. Acad. Sci. U. S. A.* **111**, 21–26, (2014).
18. R. Mostany and C. Portera-Cailliau, "A craniotomy surgery procedure for chronic brain imaging," *J. Visualized Exp.* **12**, e680 (2008).
19. S. Bahar et al., "Intrinsic optical signal imaging of neocortical seizures: the 'epileptic dip'," *Neuroreport* **17**, 499–503, (2006).

20. M. Zhao et al., "Spatiotemporal dynamics of perfusion and oximetry during ictal discharges in the rat neocortex," *J. Neurosci.* **29**, 2814–2823, (2009).
21. X. L. Dean-Ben and D. Razansky, "Functional optoacoustic human angiography with handheld video rate three dimensional scanner," *Photoacoustics* **1**, 68–73, (2013).
22. X. L. Dean-Ben and D. Razansky, "Adding fifth dimension to optoacoustic imaging: volumetric time-resolved spectrally enriched tomography," *Light Sci. Appl.* **3**, e137, (2014).
23. X. L. Dean-Ben, A. Ozbek, and D. Razansky, "Volumetric real-time tracking of peripheral human vasculature with GPU-accelerated three-dimensional optoacoustic tomography," *IEEE Trans. Med. Imaging* **32**, 2050–2055, (2013).
24. T. F. Fehm, X. L. Deán-Ben, and D. Razansky, "Four dimensional hybrid ultrasound and optoacoustic imaging via passive element optical excitation in a hand-held probe," *Appl. Phys. Lett.* **105**, 173505, (2014).
25. X. L. Dean-Ben, E. Bay, and D. Razansky, "Functional optoacoustic imaging of moving objects using microsecond-delay acquisition of multispectral three-dimensional tomographic data," *Sci. Rep.* **4**, 5878, (2014).
26. D. Razansky et al., "Multispectral opto-acoustic tomography of deep-seated fluorescent proteins *in vivo*," *Nat. Photonics* **3**, 412–417, (2009).
27. S. Tzoumas et al., "Eigenspectra optoacoustic tomography achieves quantitative blood oxygenation imaging deep in tissues," *Nat. Commun.* **7**, 12121, (2016).
28. A. Dorr, J. G. Sled, and N. Kabani, "Three-dimensional cerebral vasculature of the CBA mouse brain: a magnetic resonance imaging and micro computed tomography study," *Neuroimage* **35**, 1409–1423, (2007).
29. A. E. Dorr et al., "High resolution three-dimensional brain atlas using an average magnetic resonance image of 40 adult C57Bl/6J mice," *Neuroimage* **42**, 60–69, (2008).
30. G. Paxinos, *Paxinos and Franklin's the Mouse Brain in Stereotaxic Coordinates*, 4th ed., Academic Press, Cambridge, Massachusetts (2012).
31. Toronto Centre of Phenogenomics, Mouse Imaging Centre, Mouse Atlas, www.mouseimaging.ca/technologies/mouse_atlas/ (September 2016).
32. R. B. Buxton, "Dynamic models of BOLD contrast," *Neuroimage* **62**, 953–961 (2012).
33. P. Beard, "Biomedical photoacoustic imaging," *Interface Focus* **1**, 602–631, (2011).
34. M. Mancini et al., "Head and neck veins of the mouse. a magnetic resonance, micro computed tomography and high frequency color Doppler ultrasound study," *PLoS One* **10**, e0129912, (2015).
35. F. B. Neubauer, A. Sederberg, and J. N. MacLean, "Local changes in neocortical circuit dynamics coincide with the spread of seizures to thalamus in a model of epilepsy," *Front. Neural Circuits* **8**, 101, (2014).
36. M. Minlebaev et al., "Early gamma oscillations synchronize developing thalamus and cortex," *Science* **334**, 226–229, (2011).
37. P. S. Pearce et al., "Spike-wave discharges in adult Sprague-Dawley rats and their implications for animal models of temporal lobe epilepsy," *Epilepsy Behav.* **32**, 121–131, (2014).
38. S. Harris et al., "Contralateral dissociation between neural activity and cerebral blood volume during recurrent acute focal neocortical seizures," *Epilepsia* **55**, 1423–1430, (2014).
39. T. P. Santisakultarm and C. B. Schaffer, "Optically quantified cerebral blood flow," *J. Cereb. Blood Flow Metab.* **31**, 1337–1338, (2011).
40. M. Zhao et al., "Preictal and ictal neurovascular and metabolic coupling surrounding a seizure focus," *J. Neurosci.* **31**, 13292–13300, (2011).

Sven Gottschalk researches at the Institute for Biological and Medical Imaging (IBMI) in Munich on the development of biomedical applications of state of the art multispectral optoacoustic tomography and microscopy systems. He is currently interested in functional optoacoustic neuroimaging and the application of novel imaging probes and contrast agents for optoacoustic imaging.

Thomas Felix Fehm graduated with distinction in physics from the Technical University of Munich and University of Illinois in Urbana-Champaign. He is currently working toward a doctoral degree at the Technical University of Munich and Helmholtz Center Munich. His main research interests are in the development of new hybrid optoacoustic and ultrasound imaging approaches and multiscale image reconstruction and processing.

Xosé Luís Deán Ben received the diploma and PhD degrees in automatics and electronics engineering from the Universidade de Vigo in 2004 and 2009, respectively. Since 2010 he serves as a postdoctoral fellow at the Lab for Optoacoustics and Molecular Imaging Engineering at the Institute for Biological and Medical Imaging (IBMI), Helmholtz Center Munich. His major research interests are the development of new optoacoustic systems for preclinical and clinical applications and the elaboration of mathematical algorithms for fast and accurate imaging performance.

Vassiliy Tsytsarev holds a PhD in neuroscience from Saint-Petersburg State University, Russia. Soon after graduation he moved to Japan and spent seven years researching at the Brain Science Institute of RIKEN and Kyoto University. He then moved to the United States and is now working at the University of Maryland on functional brain mapping, neural circuits, and different types of optical brain imaging.

Daniel Razansky is professor of molecular imaging engineering at the Technical University of Munich and Helmholtz Center Munich. He earned his degrees in electrical and biomedical engineering from the Technion—Israel Institute of Technology and completed postdoctoral training in bioimaging at the Harvard Medical School. His Lab focuses on the development of biomedical imaging tools to enable imaging with high spatial and temporal resolution on different scales, from organ to cell.